High-Gain Pattern Reconfigurable MIMO Antenna Array for Wireless Handheld Terminals

Nowrin Hasan Chamok, *Student Member, IEEE*, Mustafa Harun Yılmaz, Hüseyin Arslan, *Fellow, IEEE*, and Mohammod Ali, *Senior Member, IEEE*

Abstract—The analysis, design, experimental development, and test results of a high-gain pattern reconfigurable antenna array are presented. Unlike traditional phased arrays, the proposed array has a compressed footprint making it suitable for handheld device applications. The array pattern is reconfigured at 0°, 70°, and 290° in the azimuth plane with the help of low loss RF switches while the utilization of a collinear geometry allows narrow elevation plane beamwidth and high peak gain (between 9.7 and 11 dBi using FR4 material). System level analysis shows about 59% increase in signal-to-interference-plus-noise ratio level compared to omnidirectional antennas.

Index Terms—Array, handheld, multiple-input multiple-output (MIMO), pattern reconfigurable, smart antenna.

I. Introduction

MULTIPLE-INPUT multiple-output (MIMO) wireless systems are defined as systems that comprise multiple antenna elements at both the transmitter and receiver ends [1]. MIMO offers important advantages over conventional antennas both in terms of data reliability and data capacity [2]. Considered as one of the most promising candidates of future smart antenna systems, MIMO has already been adopted for IEEE 802.11n [3], worldwide interoperability for microwave access [4], [5], and long-term evolution [6].

MIMO for handhelds is an important research area that has the potentials to bring significant advances on antenna and antenna array designs that can be housed within the smaller form factor of a mobile handheld terminal, such as a smartphone or a tablet (iPad). Traditional antennas that are frequently used in handheld devices are fixed beam antennas such as planar inverted-F antennas (PIFAs) [7]–[11] and monopole antennas [12]–[14].

These are inefficient antennas, because due to low antenna gain and lack of pattern reconfiguration capability, much

of the radiated RF power is absorbed by the head or the body resulting in wasted battery power. Furthermore, losses due to multipath fading result in signal degradation or loss. To circumvent the fading problem, *diversity* [15]–[18] have been proposed. Research has shown that only using diversity in a handheld unit signal-to-noise ratio (SNR) improvement of over 8–10 dB can be achieved [18]. This increase in SNR in turn decreases the bit-error-rate [19] resulting in improved spectral efficiency.

MIMO for the handheld [20]–[22] offers great deal of flexibility especially if it can be combined with high gain and pattern reconfiguration. Other MIMO antenna examples include [23]–[25].

The focus of this paper is to introduce a smaller form factor high-gain pattern reconfigurable MIMO antenna array for handheld terminals. The array is designed and developed using the concept of parasitic arrays [26]–[33] where a driven and one or more closely coupled parasitic elements work in tandem to allow pattern reconfiguration. Since the parasitic elements can be brought very close to the driven antenna element, the form factor of the array will be much smaller compared to a traditional phased array making them more suitable for handheld device applications. Although many articles have been published in the literature on parasitic arrays that address dipole or monopole antennas for base stations [27], [28], patch antenna arrays [29], [30], and dipole antenna arrays for wearable wireless applications [31]–[33], this is the first ever reported detailed work on a high-gain pattern reconfigurable collinear parasitic array for the handheld to the best of our knowledge. Very preliminary results of this paper were presented at a conference recently [34]. This paper presents more significant design, analysis, and experimental results and system level simulation results.

The application domain for the proposed array is illustrated in Fig. 1(a). It is a collinear array of dipole antennas arranged at one edge of a handheld terminal. Although proposed here for handheld terminal, the concept is valid for many other applications. The proposed antenna array offers two important features: it can steer the beam in three different directions, and has high gain with narrow *e* plane beamwidth. High gain is achieved by employing the collinear array geometry consisting of multiple "subarrays" that allow narrow *e* plane beamwidth. Pattern reconfiguration, on the other hand, is achieved with the help of the parasitic array idea which can be explained with the help of one subarray. Each subarray contains
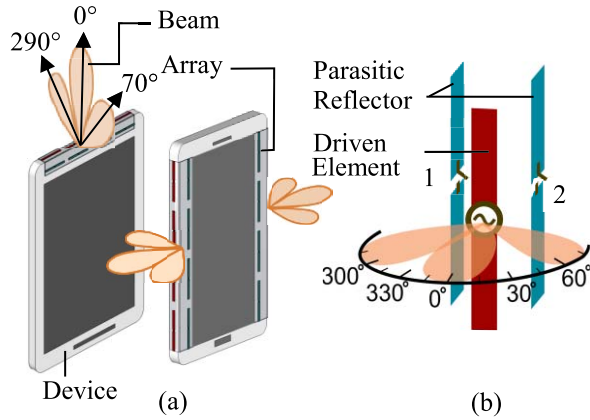
Fig. 1. (a) Conceptual drawings for the application domain of the proposed array: array at the top and side edges of the device. (b) Illustration of the working principle of the proposed pattern reconfigurable array.

three dipole elements—one driven and two parasitic [Fig. 1(b)]. The parasitic dipoles function as reflectors once activated using RF switches that are located at their centers. This allows array pattern reconfiguration in three different directions for three cases. For example, when switch 1 is ON, the parasitic on the left works as a reflector making the beam point at $\varphi = 70°$, when switch 2 is ON, the parasitic on the right works as a reflector making the beam point at $\varphi = 290°$, and when both switches 1 and 2 are ON, both parasitics work as reflectors and the beam points at $\varphi = 0°$.

The operating frequency considered here is the 5-GHz WLAN band. The rapid growth and interest in mm wave frequencies and massive MIMO will allow much larger arrays to be implemented using this concept in a variety of application scenarios, e.g., handhelds and base stations, stationary device to device, and chip to chip in computer systems.

This paper is organized as follows. First, the array configuration parameters are defined. Preliminary simulation studies are performed considering the array implementation in free space where the effects of parameters, such as the interelement distances and spacing between subarrays on array input return loss and mutual coupling, are investigated. Upon selection of appropriate design parameters, array models with implementation scopes in free space and on FR substrates are developed and analyzed both in terms of S-parameters and radiation patterns. Next, measured S-parameter results and radiation pattern characteristics of the array are presented followed by system level simulations demonstrating performance under communication scenarios.

II. ARRAY CONFIGURATION

A. Collinear Array

The geometry and dimensions of the array are shown in Fig. 2(a). There are n subarrays with the edge to edge separation between two consecutive subarrays being s. The length of the array is L. The array axis is the z-axis for our analysis with the beam pointing orthogonal to the axis. With increasing n or s, the e plane beamwidth decreases resulting in increased directivity. The choice of n and s is determined
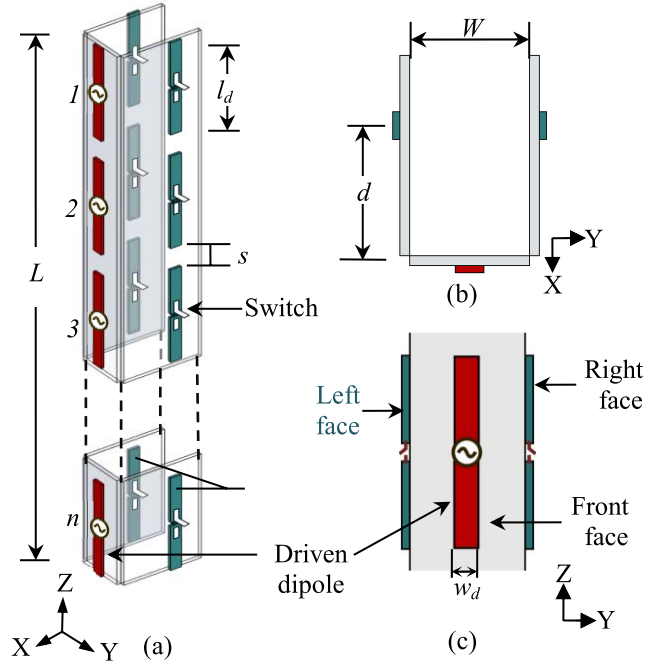

Fig. 2. (a) Proposed array geometry, (b) top view, and (c) front view of a single subarray. l_d is the dipole length. W_d is the dipole width.

primarily by the space available in terms of the operating wavelength. The parameter, s is also critical as it governs the coupling between two consecutive subarrays.

B. Subarray

As stated, a single subarray [Fig. 2(b) and (c)] consists of one driven and two parasitic elements. Planar dipole elements on three planar surfaces each approximately half-wavelength long at the operating frequency are considered. The driven element is on the yz plane labeled "Front face" [Fig. 2(c)]. The parasitic elements are on two xz planes labeled "Left face" and "Right face," respectively. The left and right faces are separated by distance, W. The distance between the driven and the parasitic is d [Fig. 2(b)]. The Front, Left, and Right faces could be considered to constitute the edge of a handheld device.

C. Operation of the Subarray

The driven element is fed using a 50-Ω source at its center. The parasitic elements contain RF switches at their centers. Consider the operation of one of the parasitic elements. With the switch OFF, each piece of the parasitic is electrically too small to have any effect on the antenna. With the switch ON, currents are induced in the parasitic. Following [31], the voltages and currents in the driven and parasitic elements are related by the impedance (Z) matrix given in (1)

$$\begin{bmatrix} V_1 \\ I_2 X \end{bmatrix} = \underbrace{\begin{bmatrix} Z_{11} & Z_{12} \\ Z_{21} & Z_{22} \end{bmatrix}}_{Z \text{ matrix}} \begin{bmatrix} I_1 \\ I_2 \end{bmatrix} \tag{1}$$

and

$$\alpha_{21} = \left(\frac{I_2}{I_1}\right) = \frac{-Z_{21}}{(Z_{22} - X)} \quad (2)$$

where the subscripts 1 and 2 correspond to the driven element and the parasitic element, respectively. The parameters Z_{NN} and the Z_{MN} are the self and mutual impedances in the Z matrix. The excitation voltage in the driven element is V_1. Clearly, Z_{MN} will strongly depend on the distance, d [Fig. 2(b)]. Once the (Z) matrix is calculated, (2) should be used to determine the magnitude and phase of the coupling coefficient, α_{21}. The phase angle of α_{21} determines if a certain parasitic element will act as a reflector or director; reflector if phase is positive and director if phase is negative [35]. The magnitude of α_{21} will affect the impedance matching of the array. If the parasitic elements are controlled using RF switches or varactor didoes, then the X in (2) should represent the equivalent circuit to represent its ON- and OFF-states.

III. MODELING DETAILS AND SIMULATION RESULTS

A. Array in Free Space

Initially, the array was designed for operation in free space in order to obtain a clear understanding of the effects of dielectric loss for the array. Given that material choices can vary, e.g., flexible film, plastics, low loss microwave materials, and FR4. performance data in free space will serve as a benchmark for comparison. Thus, the surfaces on which the dipole elements reside in Fig. 2(a) are considered to be nondielectric ($\varepsilon_r = 1.0$, $\tan\delta = 0$). As mentioned, the design frequency was 5 GHz.

The array presented in this paper consists of four subarrays, i.e., $n = 4$; hence, there are four driven elements and eight parasitic elements. The parasitics are controlled using discrete RF switches. The choice of $n = 4$ was governed by a device that is about 150-mm long. The length and width of each planar dipole element were 25.4 and 2 mm, respectively. The parameter W was selected to be 10 mm considering it to be representative of the thickness of a typical handheld device. In addition, we will select the distance, d such that the parasitic elements function as reflectors. Simulations were performed using Ansys HFSS to optimize the array design. To represent the ON-state, each switch was modeled using a 5-pF capacitor that represented the equivalent dc blocking capacitance for the switch. To represent the OFF-state, each switch was modeled using a 0.1-pF capacitor that represented the 8-dB isolation for the switch at this frequency.

Preliminary simulations were performed to select the parameters, d and s such that they allow the parasitics to work as reflectors, provide good impedance matching, and low mutual coupling. For these simulations, all switches on the parasitics were modeled as ON. First, s was kept constant at 14 mm ($3\lambda/4$ center to center distance between two consecutive subarrays) and d was varied. A set of simulations were performed varying d from 2 to 18 mm. These simulation results showed that for $d < 2$ mm, the parasitic elements worked as directors. Since we wanted the parasitic elements to work as reflectors, it was concluded that $d > 2$ mm. Important things to consider
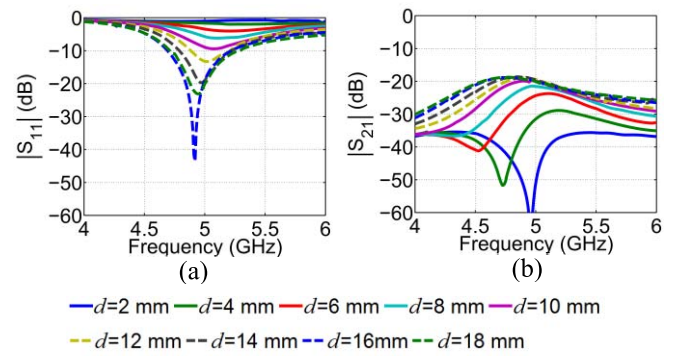

Fig. 3. Effects on S-parameter with variation of d with All switches ON.
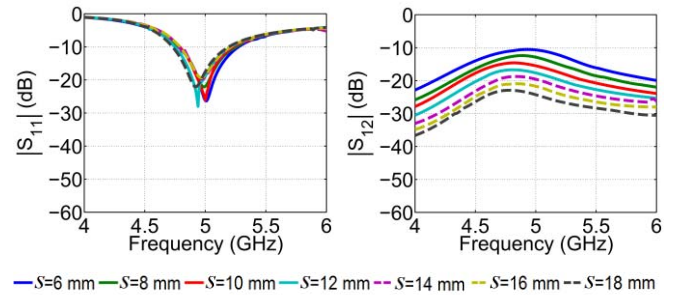

Fig. 4. Effects on S-parameter with variation of s with All switches ON.

after this was the $|S_{11}|$ response of each array and the mutual coupling between two consecutive arrays as function of d. Therefore, $|S_{11}|$ for subarray 1 and the coupling between subarrays 1 and 2 were studied as functions of frequency, given that the coupling between two consecutive subarrays is the highest. The results presented in Fig. 3 show that for $d \geq 12$ mm, $|S_{11}| < -10$ dB, and $|S_{21}| < -18$ dB. In order to obtain even better $|S_{11}|$ performance, $d = 14$ mm was selected.

Next, while d was fixed at 14 mm, s was varied from 6 to 18 mm. As can be seen from Fig. 4, $|S_{11}|$ does not vary much with s, but $|S_{21}|$ does. For the initially assumed value of s (14 mm), the $|S_{21}|$ is around -20 dB at 5 GHz, so this value was kept unchanged.

B. Computed S-Parameters for Array in Free Space

The array with $d = 14$ mm and $s = 14$ mm was then analyzed for three switching cases: Left switches ON, Right switches ON, and All switches ON. The simulated S-parameters as functions of frequency are shown in Fig. 5. The array shows overall satisfactory S-parameters: $|S_{nn}|$ ($n = 1, 2, 3, 4$) < -15 dB and $|S_{mn}|$ ($m, n = 1, 2, 3, 4$; $m \neq n$) < -15 dB.

C. Simulated Radiation Patterns for Array in Free Space

Simulated array realized gain patterns at 5 GHz in the h plane (xy) and the e plane (xz) are shown in Fig. 6(a) and (b), respectively. As seen from Fig. 6(a), the pattern has its peak at 0° when All switches are ON, at 30° when the Left switches are ON, and at 330° when the Right switches are ON. The e plane
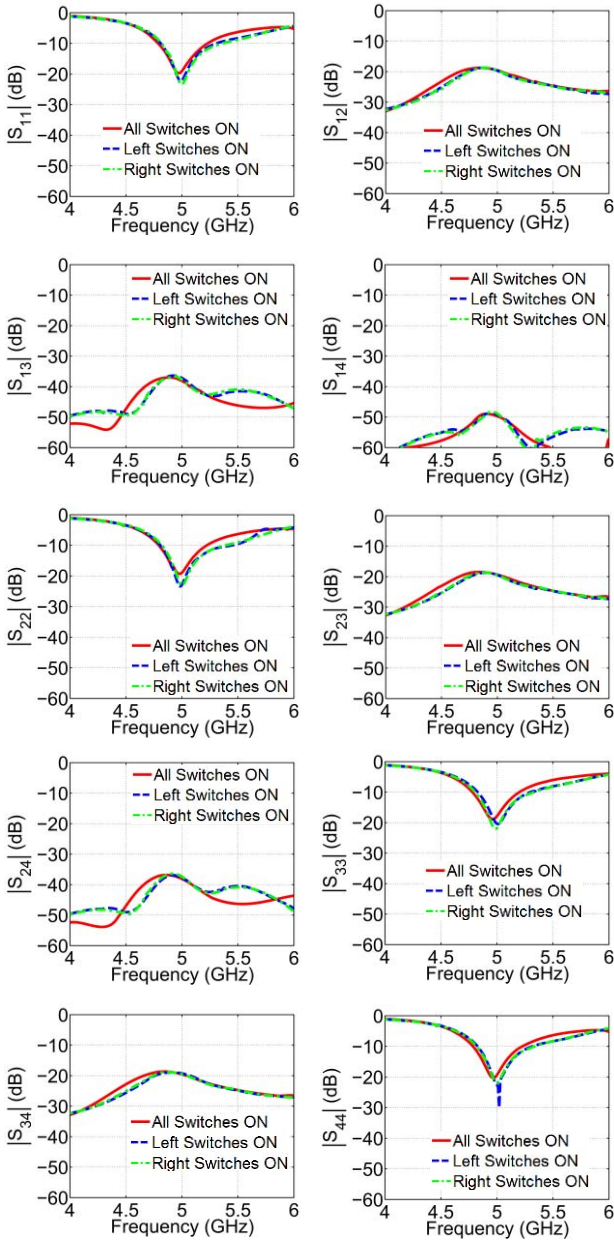
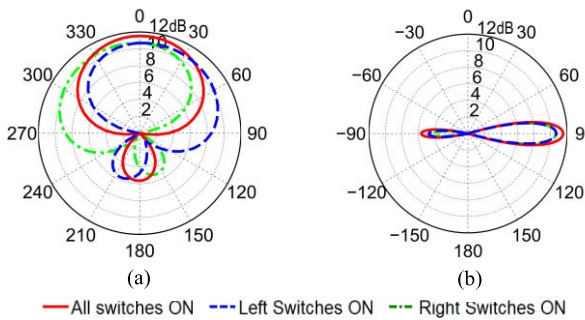Fig. 5.   Simulated S-parameters versus frequency for array in free space.

TABLE I
ARRAY PARAMETERS FOR ARRAY ON FR4

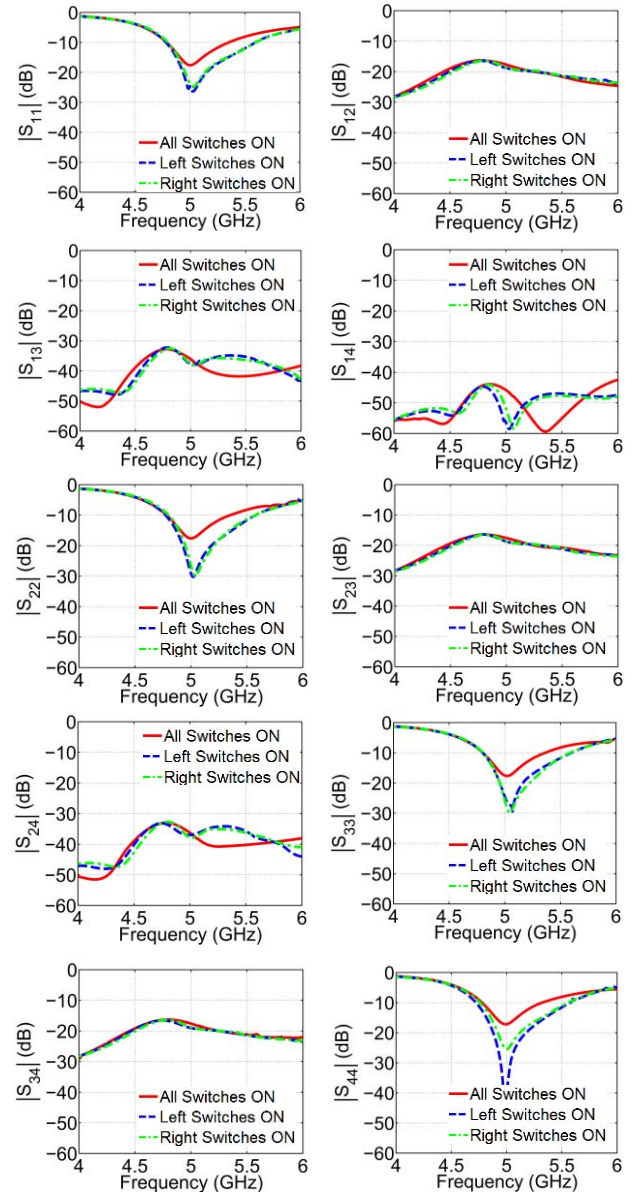| Parameter	l_d	w_d	L	W	d	s
Values (mm)	20.2	2	122.8	10	14	14

Fig. 7.   Simulated S-parameters versus frequency for array on FR4.

D. Array on FR4

In order to be able to experimentally fabricate and test an array, the free-space design was slightly modified. For the driven and parasitic dipoles on the various faces [Fig. 2(a)], three separate 0.8-mm-thick FR4 substrates ($\varepsilon_r = 4.5$, $\tan\delta = 0.02$) were considered. Dipole lengths were reduced from 25.4 to 20.2 mm in order to not change the operating frequency significantly. All other parameters were unchanged. The parameters for the array on FR4 are listed in Table I. The simulated S-parameters for this array as functions of frequency are shown in Fig. 7. It is apparent that the array operates

Fig. 6.   Computed realized gain patterns in free space in (a) *h* plane (*xy*) and (b) *e* plane (*xz*).

pattern shows a narrow beam [18° half-power beamwidth (HPBW)] as expected. The HPBW in the *h* plane is 120°. The peak gain ranges from 10.7 to 11.7 dBi.

(a)　　　　　　　(b)

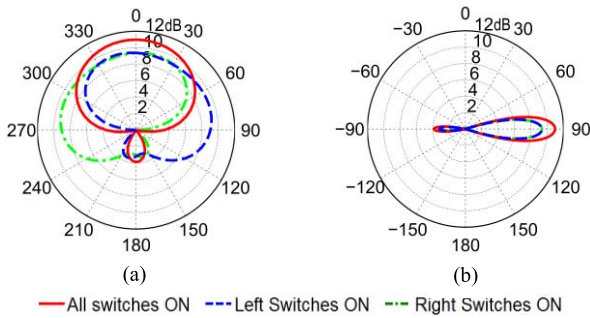— All switches ON　--- Left Switches ON　-·- Right Switches ON

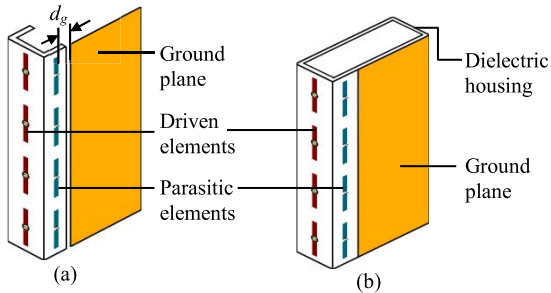Fig. 8.　Computed realized gain patterns for the array on FR4 in (a) h plane (xy) and (b) e plane (xz).

Fig. 9.　Configuration of the array with (a) ground plane and (b) ground plane and dielectric housing (not drawn to scale).

at 5 GHz with $|S_{nn}|(n = 1, 2, 3, 4) < -15$ dB and $|S_{mn}|(m, n = 1, 2, 3, 4; m \neq n) < -15$ dB.

Simulated realized gain patterns for this array are shown in Fig. 8(a) and (b). Fig. 8(a) shows the h plane (xy) and Fig. 8(b) shows the e plane (xz) realized gain patterns at 5 GHz. As seen in Fig. 8(a), the pattern has its peak at $\varphi = 0°$ when All switches are ON, at $\varphi = 70°$ when the Left switches are ON, and at $\varphi = 290°$ when the Right switches are ON. The HPBW in the e plane is 20°. The HPBW in the h plane is 120°. The peak gain ranges from 9.7 to 11 dBi. The degradation in gain (about 0.7–1 dB) is due to the $\tan \delta$ of the FR4 material.

The effect of the presence of a ground plane on antenna performance was studied. A copper ground plane (150×40 mm^2) was created on the same plane as one of the parasitic antenna planes [Fig. 9(a)]. It was placed at a distance, d_g from the corresponding parasitic elements. Two cases were considered, namely, $d_g = 5$ mm and $d_g = 10$ mm. For both cases, it was found that the effect of adding a ground plane on S-parameters was insignificant. On the other hand, a tilt in the radiation patterns was visible. When the ground plane was placed next to the right parasitic elements, the peak beam directions were at $\varphi = 75°$, $\varphi = 355°$, and $\varphi = 240°$, respectively, for Left switches ON, All switches ON, and Right switches ON cases. The gain reduced by 1 dB.

The effect of a generic dielectric housing and the ground plane on the antenna was also studied. We considered a $150 \times 70 \times 10$ mm^3 dielectric housing ($\varepsilon_r = 4.4$ and $\tan \delta = 0.02$) [Fig. 9(b)]. The thickness of the dielectric material for the housing was 0.8 mm and d_g was 10 mm. It was found that the presence of the housing caused 5% lowering of
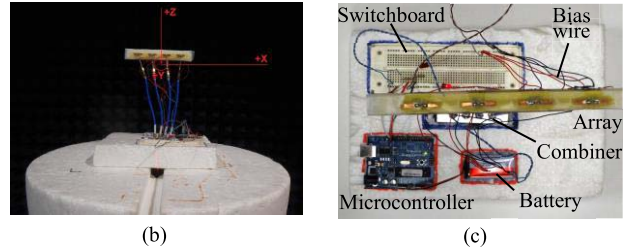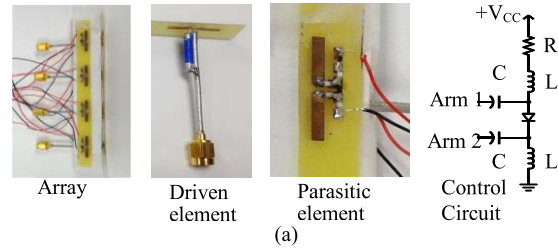

Fig. 10.　Photo of the built antenna prototype. (a) Array components and control circuit. (b) Side view and (c) top view of the setup in anechoic chamber.

the antenna center frequency. Nevertheless, the array remained operational at 5 GHz. The radiation patterns and gain were nearly identical to those obtained for the array with a ground plane.

Since the array would most likely be manufactured for placement at the edge of a mobile device, other thin, low dielectric constant, low loss materials can be used, such as plastic for example. It is unlikely that the antenna array will be made from FR4, because the device housing will not be made from FR4. Nevertheless, we think it is safe to assume that such material will be thin, have low dielectric constant and lower loss compared to FR4.

IV. EXPERIMENTAL FABRICATION AND EXPERIMENTAL RESULTS

A laboratory prototype of the array was fabricated and measured (photographs shown in Fig. 10). Each face of the array shown in Fig. 2(a) was photo-etched on a separate 0.8-mm-thick FR4 substrate. The dimension of each substrate was $145 \times 9 \times 0.8$ mm^3. Each driven dipole was fed using a 2.2-mm diameter semi-rigid 50-Ω coaxial cable and a split coax balun made from the same cable (Fig. 10). Each parasitic element was controlled using a p-i-n diode (Skyworks Inc. SMP1345) switch. The switch biasing circuit shown in Fig. 10 contains current limiting resistor, $R = 470$ Ω, inductors, $L = 10$ nH, and capacitors, $C = 10$ pF. To turn the switches ON, 5 V dc supply was applied. The application of 5 V dc results in 9 mA of forward current allowing the diode ON-state resistance to be 1.5 Ω. And thus, the expected insertion loss is 0.4 dB.

A. S-Parameter Measurements and Results

S-parameter measurements were performed for the prototype shown in Fig. 10(a). Since a two-port vector network analyzer was used at each time when the S-parameters of
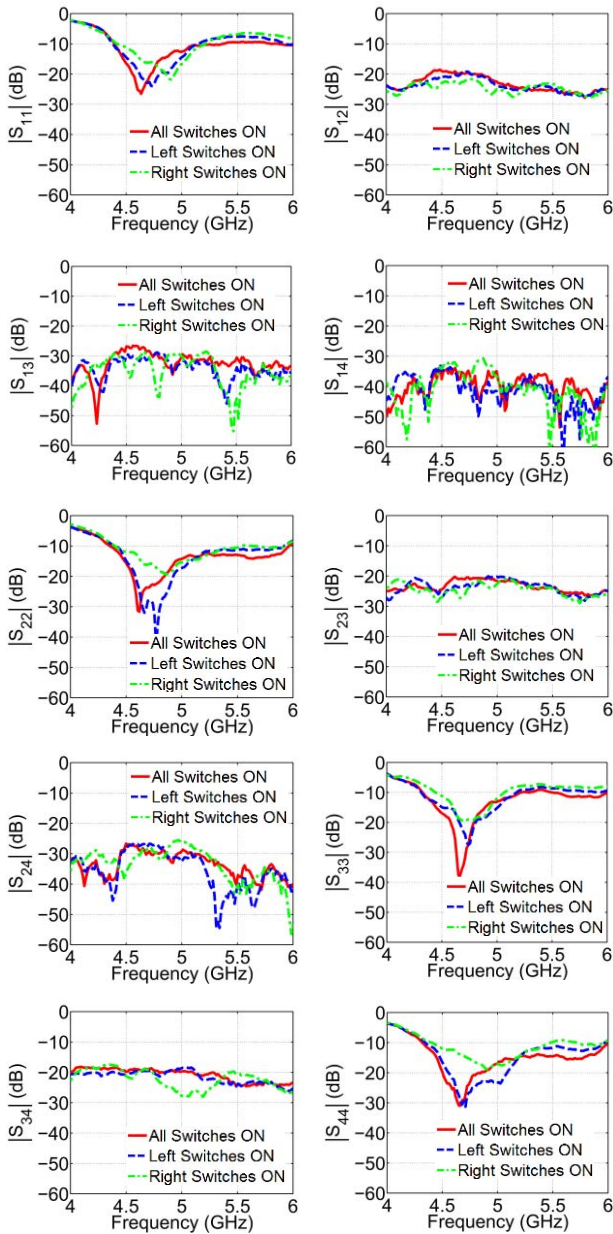
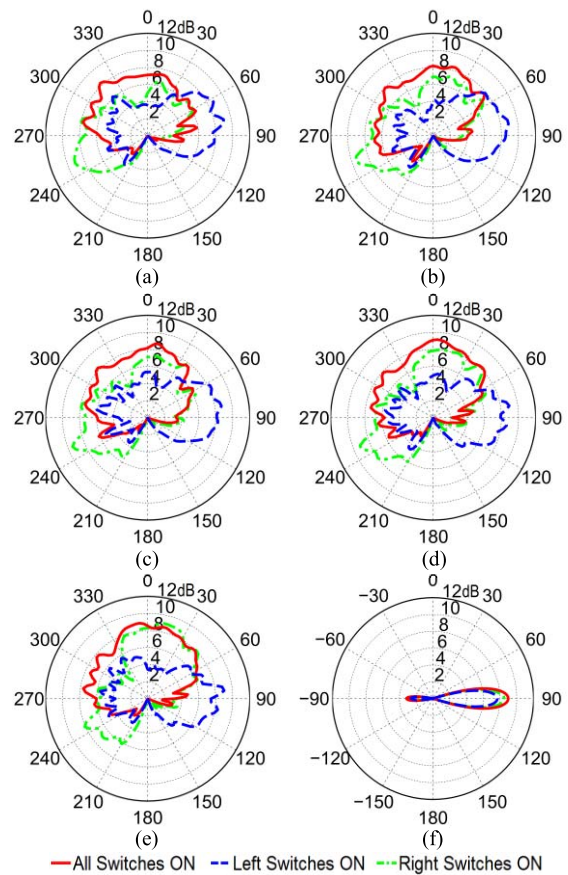Fig. 11. Measured S-parameters for the fabricated array prototype.

Fig. 12. Measured realized gain patterns in the *h* plane at (a) 4.8, (b) 4.9, (c) 5, (d) 5.1, and (e) 5.2 GHz. (f) Measured realized gain patterns in the *e* plane at 5 GHz.

two ports were measured the other two ports were terminated using 50-Ω loads. The measured S-parameter data for the array are shown in Fig. 11.

The measured results show that the array operates in the frequency range of 4.4–5.1 GHz (as $|S_{11}| \leq -10$ dB, and $|S_{21}| \leq -15$ dB is satisfied). Comparing the measured results of Fig. 10 to the simulated results of Fig. 7, it can be seen that the operating frequency for the measured is slightly lower than the simulated. The decrease in frequency is probably due to a combined effect of imperfections in the fabrication process, nonideality of FR4 material, and the adverse effect of long bias wires which were used to supply dc voltage to the switch control circuit.

B. Gain and Pattern Measurement Results

The array gain and radiation patterns were measured in a SATIMO anechoic chamber. The setup is shown in Fig. 10(b).

As shown in Fig. 10(a) and (b), each driven dipole is first connected to a split-coax balun and a coaxial cable. The balun resides between two pieces of foam, each 5-mm thick. This coaxial cable then connects to another 152.4-mm-long coaxial cable via a female-female SMA adapter. This cable assembly along with three similar assemblies from the other three driven dipoles are then connected to the four output ports of a 4-to-1 combiner (Minicircuits ZN4PD-642W-S+). The input of the combiner is connected to the measurement cable of the chamber.

A microcontroller (Arduino Duemilanova) fed by a 9 V battery was used to control the bias states of all eight switches. The 16 pieces of 381-mm-long dc bias wires were connected from the parasitic elements to the microcontroller circuit board. The assembly is shown in Fig. 10(c).

The cables, connectors, adapters, and the combiner were measured to quantify the combined insertion loss for the pattern and gain measurement setup that preceded the array elements. The insertion loss was between 1.1 and 1.3 dB. The insertion loss was added to the measured gain data from the anechoic chamber.

Measured realized gain patterns at several frequencies within the operating frequency band are shown in Fig. 12. Array pattern reconfiguration in the *h* plane is apparent from Fig. 12(a)–(e). For all three cases, namely, All switches ON,

Publication	Element no.	Meas. gain (dBi)	Freq. of operation (GHz)	Size (mm³)	Steering angles (degree)
Qin *et al.* [21]	2	6	5.2	30×30 ×30.2	Not well-defined
Kishor and Hum[20]	4	2.5	2.3	90×30× 5	30, -30
Rhee *et al.* [22]	4	5.4	5.2	120×40 ×6	30, -30
Proposed array	4	10	5	123×10 ×14	70,0, 290

Left switches ON, and Right switches ON measured peak gain is between 8 and 10 dBi. Measured antenna efficiency is about 80%. The individual patterns for the three cases provide a near hemispherical coverage with an average array gain of 8 dBi. The HPBW for the All ON case is wider than the HPBW for the other cases. Average HPBW is about 100°. The *e* plane patterns for one frequency shown in Fig. 12(f) show that the beams are narrower as expected with the HPBW of about 25°. Comparing the measured patterns of Fig. 12 with the simulated patterns shown in Fig. 8, there are signs of reflections and distortions in the measured patterns. These are more pronounced for the case called the Right switches ON. Ideally, the *h* plane patterns should be directed at 0°, 70°, and 290° for the All ON, Left ON, and Right ON cases, respectively. Measured patterns for the Right ON appear to be rotated.

The differences between the simulated and measured patterns can be attributed to the presence of the four coaxial cables and split coax baluns, the 16 dc bias wires, and also possibly the power combiner that were not present in the simulation models. It is expected that if lumped element chip baluns and dc bias traces made from high resistance (>500 Ω/square) lines [36] are implemented much of the reflections and distortions in the pattern will disappear. The simulation models did not include the cables and the wires which are likely the cause for the discrepancies.

The performance (measured gain and steering angle) of the proposed array is compared against available designs in Table II. As seen, the proposed array provides higher gain and multiple steering angles which are likely to be beneficial for future handheld devices.

V. SYSTEM LEVEL PERFORMANCE ANALYSIS

A. Envelope Correlation Coefficient

Envelope correlation coefficient (ECC) is a metric often used for MIMO antennas that measures the correlation between two antennas. For MIMO applications with N antennas, the ECC between the ith and the jth elements is given by [37]

$$\rho_e(i, j, N) = \frac{\left|\sum_{n=1}^{N} S_{i,n}^* S_{n,j}\right|^2}{\prod_{k=i,j}\left(1 - \sum_{n=1}^{N} S_{k,n}^* S_{n,k}\right)}. \quad (3)$$

Fig. 13 shows the ECC for the array that was computed using the measured S-parameter data presented in Fig. 11. As seen, ECC < 0.01 which is excellent for an MIMO array. Note that
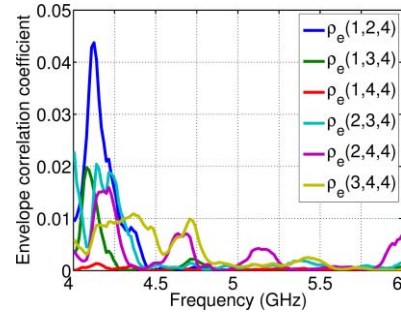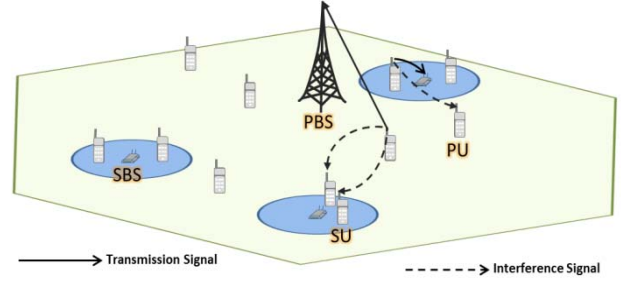

Fig. 13. ECC from measured data.

Fig. 14. Heterogeneous network structure with PUs, SUs, and secondary base stations within a primary cell with a primary base station.

for accurate ECC calculation, instead of S-parameters far-field patterns should be used since the former considers lossless antennas [38]. However, for efficient antennas, S-parameter-based ECC calculation method yields good results [39].

B. Signal-to-Interference-Plus-Noise Ratio Performance

Finally, a system level analysis is performed to understand the performance characteristics of the proposed array compared to two other antennas: a 5-dBi gain omnidirectional antenna and an MIMO array proposed by Kishor and Hum [20] which has two states. Resource allocation study is carried out among the secondary users (SUs) within the game theoretical framework in the heterogeneous networks which consist of 16 primary users (PUs) and 20 secondary base stations with two SUs in each under one primary network (Fig. 14). We consider that the number of available resources is 256 under the orthogonal frequency division multiple accessing scheme, and it is assumed that all resources are allocated by PUs. Likewise, the SUs in each secondary network are considered to use all resources. Since the aim is to decrease the interference induced on the PUs, only SUs are assumed to use the array by Kishor and Hum [20] or the proposed array, i.e., PUs are equipped with only omnidirectional antennas. Signal-to-interference-plus-noise ratio (SINR) of an SU u can be expressed as follows:

$$\text{SINR}_u = \sum_{f \in F} \frac{p_u g_{uf} \beta_{uf}}{\sum_{\substack{v \in U, \\ v \neq u}} p_v g_{vf} \beta_{vf} + \sum_{b \in B} p_b g_{bf} \beta_{bf} + \omega_0} \quad (4)$$

where $f = 1, 2, \ldots, F$ is the subcarrier index, U and B show the total number of SUs and PUs, respectively, v is the interfering SU index, $u, v \epsilon U$, b is the PU index, p_u denotes the transmit power for user u, and parameter β_{uf} is the indicator
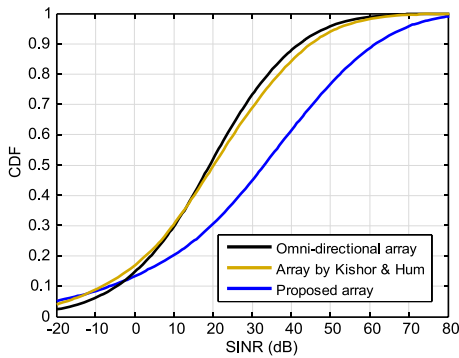
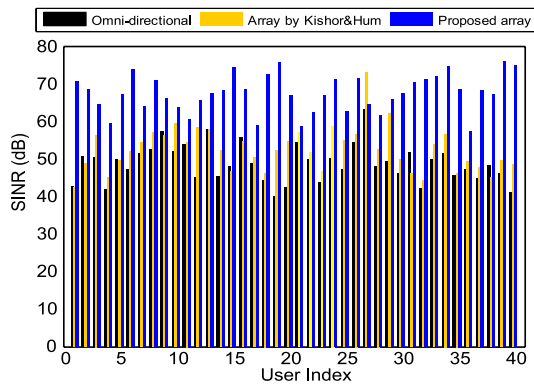Fig. 15.　Comparison of the proposed array with omnidirectional antenna and array by Kishor and Hum [20].

Fig. 16.　Mean SINR gain of each SU.

function for the fth subcarrier. If SU u uses the fth subcarrier, $\beta_{uf} = 1$, otherwise $\beta_{uf} = 0$. ω_0 is the additive white Gaussian noise.

Fig. 15 shows the performance results of the proposed array, omnidirectional antenna, and the array by Kishor and Hum in terms of SINR. As seen from Fig. 15, proposed array outperforms the standard antennas. While 50% of the SINR values are only below 19 and 20 dB for the omnidirectional antenna and the Kishor and Hum [20] antenna, respectively, 50% of the SINR values are below 33 dB for our proposed array. In other words, the gain in mean SINR of the Kishor and Hum antenna over the omnidirectional antenna is 2.5%. The same for the proposed antenna over an omnidirectional antenna is 59%. This indicates that the SUs can achieve higher SINR values with proposed array. This result can also be confirmed from Fig. 16 which shows the mean SINR gain obtained in each SU. As shown in Fig. 16, almost every SU achieves higher gain with proposed array. System level results indicate that the proposed array is a strong candidate for the user devices in heterogeneous networks.

VI. CONCLUSION

A four-subarray collinear pattern reconfigurable smart antenna array was designed, developed, and tested validating performance. Simulation results in both free space and on FR4 show that the array operates at around 5 GHz with better than 10-dB return loss and better than 17-dB mutual coupling. For the FR4 array, the peak gain is between 9.7 and 11 dBi for the

three different reconfiguration angles, e.g., $0°$, $70°$, and $290°$. Experimental fabrication and tests show that the array meets the input $|S_{nn}|$ and $|S_{mn}|$ characteristics of <-10 dB and <-15 dB, respectively.

Measured pattern results show the pattern reconfiguration in three different angles in the azimuth albeit with some degradation due to the presence of long dc bias wires. Measured peak gain is about 1 dB lower than the simulated gain. The reflections and distortions in the pattern can be largely eliminated by the use of lumped element baluns and dc bias traces made from materials with high sheet resistance (>500 Ω/square for instance) as opposed to standard copper wires. However, in that case, instead of p-i-n diodes that are current (mA) controlled varactor diodes or RF MEM switches should be used that almost conduct no current ($<$nA). Finally, when the radiation properties and gain results were used in system level simulations, it was found that the high-gain pattern reconfigurable antenna array provided 59% increase in SINR over an omnidirectional antenna.

REFERENCES

[1] D. Gesbert, M. Shafi, D. Shiu, P. J. Smith, and A. Naguib, "From theory to practice: An overview of MIMO space-time coded wireless systems," *IEEE J. Sel. Areas Commun.*, vol. 21, no. 3, pp. 281–302, Apr. 2003.

[2] A. F. Molisch and M. Z. Win, "MIMO systems with antenna selection," *IEEE Commun. Mag.*, vol. 5, no. 1, pp. 46–56, Mar. 2004.

[3] A. Yavanoğlu and O. Ertuğ, "On the capacity analysis of IEEE802.11n MIMO-OFDM WLAN systems using sub-optimal MIMO detectors and compact space-multimode antenna arrays," in *Proc. 3rd Int. Congr. Ultra-Modern Telecomm. Control Syst. Workshops (ICUMT)*, 2011, pp. 1–6.

[4] Q. Li, X. E. Lin, J. Zhang, and W. Roh, "Advancement of MIMO technology in WiMAX: From IEEE 802.16d/e/j to 802.16m," *IEEE Commun. Mag.*, vol. 47, no. 6, pp. 100–107, Jun. 2009.

[5] E. Kurniawan, A. S. Madhukumar, and F. Chin, "Performance analysis of MIMO enabled broadband wireless access system for mobile multimedia applications," in *Proc. 5th Int. Conf. Inf. Commun. Signal Process.*, 2005, pp. 941–945.

[6] G. Liu, J. Zhang, P. Zhang, Y. Wang, X. Liu, and S. Li, "Evolution map from TD-SCDMA to FuTURE B3G TDD," *IEEE Commun. Mag.*, vol. 44, no. 3, pp. 54–61, Mar. 2006.

[7] K.-L. Wong, *Planar Antennas for Wireless Communications*. New York, NY, USA: Wiley, 2003.

[8] K. L. Virga and Y. Rahmat-Samii, "Low-profile enhanced-bandwidth PIFA antennas for wireless communications packaging," *IEEE Trans. Microw. Theory Techn.*, vol. 45, no. 10, pp. 1879–1888, Oct. 1997.

[9] M. F. Abedin and M. Ali, "Modifying the ground plane and its effect on planar inverted-F antennas (PIFAs) for mobile phone handsets," *IEEE Antennas Wireless Propag. Lett.*, vol. 2, no. 1, pp. 226–229, 2003.

[10] C.-T. Lee and K.-L. Wong, "Uniplanar printed coupled-fed PIFA with a band-notching slit for WLAN/WiMAX operation in the laptop computer," *IEEE Trans. Antennas Propag.*, vol. 57, no. 4, pp. 1252–1258, Apr. 2009.

[11] H. T. Chattha, M. Nasir, Q. H. Abbasi, Y. Huang, and S. S. Alja'afreh, "Compact low-profile dual-port single wideband planar inverted-F MIMO antenna," *IEEE Antennas Wireless Propag. Lett.*, vol. 12, pp. 1673–1675, 2013.

[12] M. Ali, G. J. Hayes, H.-S. Hwang, and R. A. Sadler, "Design of a multiband internal antenna for third generation mobile phone handsets," *IEEE Trans. Antennas Propag.*, vol. 51, no. 7, pp. 1452–1461, Jul. 2003.

[13] K. M. Z. Shams and M. Ali, "Study and design of a capacitively coupled polymeric internal antenna," *IEEE Trans. Antennas Propag.*, vol. 53, no. 3, pp. 985–993, Mar. 2005.

[14] D. A. Ketzaki and T. V. Yioultsis, "Metamaterial-based design of planar compact MIMO monopoles," *IEEE Trans. Antennas Propag.*, vol. 61, no. 5, pp. 2758–2766, May 2013.

[15] J. S. Colburn, Y. Rahmat-Samii, M. A. Jensen, and G. J. Pottie, "Evaluation of personal communications dual-antenna handset diversity performance," *IEEE Trans. Veh. Technol.*, vol. 47, no. 3, pp. 737–746, Aug. 1998.

[16] M. Z. Azad and M. Ali, "A new class of miniature embedded inverted-F antennas (IFAs) for 2.4 GHz WLAN application," *IEEE Trans. Antennas Propag.*, vol. 54, no. 9, pp. 2585–2592, Sep. 2006.

[17] A. T. M. Sayem, S. Khan, and M. Ali, "A miniature spiral diversity antenna system with high overall gain coverage and low SAR," *IEEE Antennas Wireless Propag. Lett.*, vol. 8, pp. 49–52, 2009.

[18] C. B. Dietrich, Jr., K. Dietze, J. R. Nealy, and W. L. Stutzman, "Spatial, polarization, and pattern diversity for wireless handheld terminals," *IEEE Trans. Antennas Propag.*, vol. 49, no. 9, pp. 1271–1281, Sep. 2001.

[19] L. Vallozzi, P. Van Torre, C. Hertleer, H. Rogier, M. Moeneclaey, and J. Verhaevert, "Wireless communication for firefighters using dual-polarized textile antennas integrated in their garment," *IEEE Trans. Antennas Propag.*, vol. 58, no. 4, pp. 910–918, Apr. 2010.

[20] K. Kumar Kishor and S. V. Hum, "A pattern reconfigurable chassis-mode MIMO antenna," *IEEE Trans. Antennas Propag.*, vol. 62, no. 6, pp. 3290–3298, Jun. 2014.

[21] P.-Y. Qin, Y. J. Guo, A. R. Weily, and C.-H. Liang, "A pattern reconfigurable U-slot antenna and its applications in MIMO systems," *IEEE Trans. Antennas Propag.*, vol. 60, no. 2, pp. 516–528, Feb. 2012.

[22] C. Rhee *et al.*, "Pattern-reconfigurable MIMO antenna for high isolation and low correlation," *IEEE Antennas Wireless Propag. Lett.*, vol. 13, no. 6, pp. 1373–1376, 2014.

[23] I. Khan, I. Ullah, and P. S. Hall, "Transmit-receive diversity for 2×2 multiple-input multiple-output channel in body area networks," *IET J. Microw., Antennas Propag.*, vol. 5, no. 13, pp. 1589–1593, Oct. 2011.

[24] M. Qaraqe, Q. H. Abbasi, A. Alomainy, and E. Serpedin, "Experimental evaluation of MIMO capacity for ultrawideband body-centric wireless propagation channels," *IEEE Antennas Wireless Propag. Lett.*, vol. 13, pp. 495–498, 2014.

[25] S. Shoaib, I. Shoaib, N. Shoaib, X. Chen, and C. G. Parini, "Design and performance study of a dual-element multiband printed monopole antenna array for MIMO terminals," *IEEE Antennas Wireless Propag. Lett.*, vol. 13, pp. 329–332, 2014.

[26] M. R. Islam and M. Ali, "Ground current modification of mobile terminal antennas and its effects," *IEEE Antennas Wireless Propag. Lett.*, vol. 10, pp. 438–441, 2011.

[27] Y. Cui, R. Li, and P. Wang, "Novel dual-broadband planar antenna and its array for 2G/3G/LTE base stations," *IEEE Trans. Antennas Propag.*, vol. 61, no. 3, pp. 1132–1139, Mar. 2013.

[28] Y. Liu, H. Yi, F.-W. Wang, and S.-X. Gong, "A novel miniaturized broadband dual-polarized dipole antenna for base station," *IEEE Antennas Wireless Propag. Lett.*, vol. 12, pp. 1335–1338, 2013.

[29] M. V. Varnoosfaderani, D. V. Thiel, J. Lu, and M. Kanesan, "Dual mode switched parasitic antenna for on/off body communication channels," in *Proc. Int. Workshop Antenna Technol., Small Antennas, Novel EM Struct. Mater., Appl. (iWAT)*, 2014, pp. 25–28.

[30] J. J. Luther, S. Ebadi, and X. Gong, "A microstrip patch electronically steerable parasitic array radiator (ESPAR) antenna with reactance-tuned coupling and maintained resonance," *IEEE Trans. Antennas Propag.*, vol. 60, no. 4, pp. 1803–1813, Apr. 2012.

[31] M. R. Islam, N. H. Chamok, and M. Ali, "Switched parasitic dipole antenna array for high-data-rate body-worn wireless applications," *IEEE Antennas Wireless Propag. Lett.*, vol. 11, pp. 693–696, 2012.

[32] M. R. Islam and M. Ali, "Body-wearable beam steering antenna array for 5.2 GHz WLAN applications," in *Proc. 7th Int. Conf. Elect. Comput. Eng. (ICECE)*, Dec. 2012, pp. 447–449.

[33] M. R. Islam and M. Ali, "A 900 MHz beam steering parasitic antenna array for wearable wireless applications," *IEEE Trans. Antennas Propag.*, vol. 61, no. 9, pp. 4520–4527, Sep. 2013.

[34] N. H. Chamok and M. Ali, "A 5 GHz beam steering array for portable wireless MIMO application," in *Proc. IEEE Antennas Propag. Soc. Int. Symp.*, Memphis, TN, USA, Jul. 2014, pp. 1656–1657.

[35] R. S. Elliott, *Antenna Theory and Design*. Piscataway, NJ, USA: IEEE Press, 2003.

[36] D. E. Anagnostou, G. Zheng, S. E. Barbin, M. T. Chryssomallis, J. Papapolymerou, and C. G. Christodoulou, "An X-band reconfigurable planar dipole antenna," in *Proc. SBMO/IEEE MTT-S Int. Conf. Microw. Optoelectron.*, Jul. 2005, pp. 654–656.

[37] J. Thaysen and K. B. Jakobsen, "Envelope correlation in (N, N) MIMO antenna array from scattering parameters," *Microw. Opt. Technol. Lett.*, vol. 48, no. 5, pp. 832–834, 2006.

[38] S. Blanch, J. Romeu, and I. Corbella, "Exact representation of antenna system diversity performance from input parameter description," *Electron. Lett.*, vol. 39, no. 9, pp. 705–707, May 2003.

[39] C. Votis, G. Tatsis, and P. Kostarakis, "Envelope correlation parameter measurements in a MIMO antenna array configuration," *Int. J. Commun., Netw. Syst. Sci.*, vol. 3, no. 4, pp. 350–354, Apr. 2010.

Nowrin Hasan Chamok (S'12) received the B.Sc. degree in electrical engineering from the Bangladesh University of Engineering and Technology, Dhaka, Bangladesh, in 2009, and the M.E. degree in electrical engineering from the University of South Carolina, Columbia, SC, USA, in 2014.

He has been a Graduate Research Assistant with the Microwave Engineering Laboratory, Department of Electrical Engineering, University of South Carolina, since 2011. He has authored or co-authored several journal and conference papers. His current research interests include the fundamental research of broadband multifunctional metamaterial, pattern reconfigurable array design for handheld terminals, and body-worn antenna design.

Mustafa Harun Yılmaz was born in Bursa, Turkey. He received the B.S. degree from the Department of Electronic and Computer Teaching, Gazi University, Ankara, Turkey, in 2007, and the M.E. degree from Southern University and A&M College, Baton Rouge, LA, USA, in 2011. He is currently pursuing the Ph.D. degree as a Graduate Research Assistant with the Department of Electrical Engineering, University of South Florida, Tampa, FL, USA.

He was with Texas A&M University at Qatar, Doha, Qatar, in 2013 and 2014. His current research interests include interference coordination, interference management, resource allocation, signal identification and physical layer security, heterogeneous networks, and cognitive radio.

Hüseyin Arslan (M'93–F'16) received the B.S. degree from Middle East Technical University, Ankara, Turkey, in 1992, and the M.S. and Ph.D. degrees from Southern Methodist University, Dallas, TX, USA, in 1994 and 1998, respectively.

He was with the research group at Ericsson Inc., Research Triangle Park, NC, USA, from 1998 to 2002, where he was involved in several projects related to 2G and 3G wireless communication systems. Since 2002, he has been with the Electrical Engineering Department, University of South Florida, Tampa, FL, USA, where he is currently a Professor. In 2013, he joined Istanbul Medipol University, Istanbul, Turkey, to found the Engineering College, where he is the Dean of the School of Engineering and Natural Sciences. He also serves the Director of the Graduate School of Engineering and Natural Sciences with Istanbul Medipol University. In addition, he was a part-time Consultant for various companies and institutions, including Anritsu Company, Morgan Hill, CA, and The Scientific and Technological Research Council of Turkey, Savronik, Turkey. His current research interests include advanced signal processing techniques at the physical and medium access layers, with cross-layer design for networking adaptivity and quality of service control, many forms of wireless technologies, including cellular radio, wireless PAN/LAN/MANs, fixed wireless access, aeronautical networks, underwater networks, *in vivo* networks, and wireless sensors networks, 5G and beyond, physical layer security, signal intelligence, cognitive radio, small cells, powerline communications, smart grid, UWB, multicarrier wireless technologies, dynamic spectrum access, coexistence issues on heterogeneous networks, aeronautical (high altitude platform) communications, *in vivo* channel modeling and system design, and underwater acoustic communications.

Dr. Arslan is a member of the Editorial Board of the IEEE TRANSACTIONS ON COGNITIVE COMMUNICATIONS AND NETWORKING, and *IEEE Communications Surveys and Tutorials*. He has also served as a member of the Editorial Board of the IEEE TRANSACTIONS ON COMMUNICATIONS, the *Elsevier Physical Communication Journal*, the *Hindawi Journal of Electrical and Computer Engineering*, and *Wiley Wireless Communication and Mobile Computing Journal*. He has served as a Technical Program Committee Chair, Technical Program Committee Member, Session and Symposium Organizer, and Workshop Chair in several IEEE conferences.

Mohammod Ali (M'93–SM'03) received the B.Sc. degree in electrical and electronic engineering from the Bangladesh University of Engineering and Technology, Dhaka, Bangladesh, in 1987, and the M.A.Sc. and Ph.D. degrees in electrical engineering from the University of Victoria, Victoria, BC, Canada, in 1994 and 1997, respectively.

From 1998 to 2001, he was with Ericsson Inc., Research Triangle Park, NC, USA. Since 2001, he has been with the Department of Electrical Engineering, University of South Carolina, Columbia, SC, USA, where he is currently a Professor. He was a Visiting Research Scientist with the Motorola Corporate EME Research Laboratory, Plantation, FL, USA, in 2004. More recently, he was a Summer Faculty Fellow with the Air Force Research Laboratory (AFRL), Wright-Patterson Air Force Base (WPAFB), Dayton, OH, USA, in 2010 and 2011. He spent a year on sabbatical leave with AFRL, WPAFB, from 2013 to 2014. He has authored or co-authored over 160 publications and holds eight U.S. patents. His specific research interests include in the fields of new active device (MEMS, GAN devices, varactors, and VO2) integration with antennas and phase shifting structures; novel materials (structural composites, fabrics, liquid metal) and their exploitation to design antennas, dc bias networks, and power supply routes; 3-D printing of metamaterials for antennas as well as radomes; RF heating or energy focusing using both low and high frequency techniques; the application of magnetic materials into RF structures for antennas, co-site interference reduction, and metamaterials; and beamforming/MIMO in the handheld and base stations for 5G and beyond. His current research interests include conformal antennas, reconfigurable antennas, broadband structural load bearing antennas, metamaterials and metasurfaces, aircraft antennas and their coupling reduction, MIMO antennas, and wireless power transfer and wireless sensors.

Dr. Ali was a recipient of the 2003 National Science Foundation Faculty Career Award. He was also a recipient of the College of Engineering and Computing Young Investigator Award, the Research Progress Award, and the Samuel Litman Distinguished Professor Award from the University of South Carolina in 2006, 2009, and 2011, respectively. He was the Technical Program Co-Chair of the IEEE Antennas and Propagation Society's International Symposium in Charleston, SC, USA, in 2009. He was an Associate Editor of the *IEEE Antennas and Wireless Propagation Letters* from 2008 to 2013. He serves on the Technical Program Committee of the IEEE Antennas and Propagation Society's (APS) International Symposium. He has organized specials session for the IEEE IWAT conference and the IEEE APS Symposia in the past. He has also served on the Technical Program Committee of the IEEE SmartGrid Conference, the European Association for Antennas and Propagation Conference, and the APMC Conference. He serves on the Editorial Boards of the *International Journal of RF and Microwave Computer-Aided Engineering* and the *International Journal of Antennas and Propagation* (Hindawi).